Materials Chemistry and Physics

Unravelling the role of TiO2 nanoparticles on the optical performance of dark colorants for coatings

--Manuscript Draft--

Manuscript Number:	
Article Type:	Full Length Article
Keywords:	Titanium Dioxide; Near-Infrared Reflectance; Black Colourant; Durability; Envelope systems
Corresponding Author:	Rita Carvalho Veloso Universidade do Porto Faculdade de Ciências Porto, Porto PORTUGAL
First Author:	Rita Carvalho Veloso
Order of Authors:	Rita Carvalho Veloso
	Catarina Dias, PhD
	Andrea Souza
	Nuno M.M. Ramos, Professor
	João Ventura, PhD
Abstract:	The growing concern on energy savings in buildings, particularly related with cooling needs, has led to the search of new constructive solutions. Frequently, darker colour coatings are used in buildings for aesthetics purposes. However, such coatings have low reflectance, absorbing a large portion of the solar radiation. The associated heat gains enhance the building cooling demand and may reduce the service life of renderings owing to the increased thermal stresses by comparison to light colour coatings. The aim of this study was to assess the influence of size (30 to 5000 nm), optical band gap energy and concentration (0-20%) of TiO2 nanoparticles in a conventional black colorant for building applications. We confirm that the use of TiO2 nanoparticles increases the reflectance of the colorant and demonstrate that 50 nm is the most adequate nanoparticle size for reflectance enhancement. Furthermore, the colorimetric parameters are also affected by TiO2 doping, with the colour difference becoming increasingly noticeable to the human eye with increasing TiO2 concentration. Such results can lead to new formulations of solar reflective coatings able to reduce the overall cooling load, particularly in warm climates with high cooling demands.
Suggested Reviewers:	Michele Zinzi michele.zinzi@enea.it
	Nicola Sangiorgi nicola.sangiorgi@istec.cnr.it

Unravelling the role of TiO_2 nanoparticles on the optical performance of dark colorants for coatings

Rita Carvalho Veloso[1,2*], Catarina Dias[1], Andrea Souza[2], Nuno M. M. Ramos[2], João Ventura[1]

[1]IFIMUP, Departamento de Física e Astronomia, Faculdade de Ciências, Universidade do Porto, Rua do Campo Alegre s/n, 4169–007 Porto, Portugal

[2]CONSTRUCT-LFC, Departamento de Engenharia Civil, Faculdade de Engenharia, Universidade do Porto, Rua Dr. Roberto Frias, 4200-465 Porto, Portugal

* corresponding author details, up201001431@up.pt

Abstract

The growing concern on energy savings in buildings, particularly related with cooling needs, has led to the search of new constructive solutions. Frequently, darker colour coatings are used in buildings for aesthetics purposes. However, such coatings have low reflectance, absorbing a large portion of the solar radiation. The associated heat gains enhance the building cooling demand and may reduce the service life of renderings owing to the increased thermal stresses by comparison to light colour coatings. The aim of this study was to assess the influence of size (30 to 5000 nm), optical band gap energy and concentration (0-20%) of TiO_2 nanoparticles in a conventional black colorant for building applications. We confirm that the use of TiO_2 nanoparticles increases the reflectance of the colorant and demonstrate that 50 nm is the most adequate nanoparticle size for reflectance enhancement. Furthermore, the colorimetric parameters are also affected by TiO_2 doping, with the colour difference becoming increasingly noticeable to the human eye with increasing TiO_2 concentration. Such results can lead to new formulations of solar reflective coatings able to reduce the overall cooling load, particularly in warm climates with high cooling demands.

Keywords: Titanium Dioxide; Near-Infrared Reflectance; Black Colourant; Durability; Envelope systems.

1. Introduction

Building components play a vital role in energy conservation or dissipation. High intensity solar radiation that reaches envelope systems (mainly roofs and façades) can lead to a large surface temperature increase. The consequent temperature rise increases energy cooling demands and thermal discomfort of building occupants, and contributes to the urban heat island effect [1, 2]. Furthermore, the increase of the exterior surface temperature increases the risk of early degradation of envelope finishing materials [3]. This is particularly important when dark or black colours are used in the exterior surfaces, driven by aesthetic reasons. In fact, conventional black colourants, usually based on carbon black or black iron oxide, have an excessive absorption of solar radiation, reflecting only approximately 5% of sunlight [4].

The use of high solar reflective coatings (so-called cool pigments) in building envelope systems is a relevant technique to reduce the environmental loads [2]. In particular, the use of near-infrared (NIR)-reflective coatings has been widely explored [5-14]. For instance, Zinzi [15] selected a variety of coloured products to be incorporated in an acrylic based masonry paint with quartz filler, typically used as finishing coating in façades, and obtained promising reflectivity results on cool coatings. They prepared a colour pattern of cool and conventional colours and compared the correspondent radiative properties. The developed coatings showed a noteworthy improvement in solar and near-infrared reflectance for dark tones (up to 0.16 and 0.38, respectively). Pisello et al. [16] combined two passive cooling strategies for building envelopes (cool façade and cool roof) showing an general temperature reduction of 3.1°C (13%). Furthermore, with the application of one high reflective component, it was possible to obtain a 19.8ºC (55%)

decrease. In addition, several studies have focused on incorporating nanomaterials in coatings, as these allow an effective control of the radiative properties through the tuning of their optical materials [17, 18]. Nevertheless, although several studies have been carried out on NIR-reflective coatings, very few have focused on the effects of particle size, shape and concentration on spectral performance, especially concerning dark or black coatings [19].

Among all nanomaterials, rutile TiO_2 is the most effective white nanopigment, improving coatings opacity, coverage power, durability, and brightness [20]. The outstanding and unique properties of TiO_2 include high refractive index, when compared with other white nanomaterials (e.g., $BaSO_4$, ZnO, ZrO_2 or $CaCO_3$) [21, 22] , or active UV protection [23], making it an optimum candidate to be used as a NIR-reflective nanomaterial [24-29]. To understand how the TiO_2 nanoparticles characteristics influence the properties of thermal insulation coatings, Shen et al. [30] varied their concentration and particle size. The results indicate an enhancement of the solar reflectance of the white coating with increasing particle content.

Although the effective influence of TiO_2 nanoparticles on the reduction of coatings solar absorption is known, previous studies typically focus on maximizing the reflectance across the entire solar spectrum without considering aesthetic effects. There have also been numerical methods and analysis models reporting the effect of the morphology of these nanoparticles on the reflective properties, but a systematic experimental study has never been performed. As such, our thorough study aims to explore the effect of size, size distribution, optical band gap and concentration of TiO_2 nanoparticles dispersed in a commercial black colourant on its optical performance. The optical performance of the doped black colourant samples was experimentally evaluated through spectral reflectance calculations using a modular spectrophotometer to

understand the relation between these properties and the intrinsic characteristics of the TiO_2 nanoparticles. We show the potential of these pigments to be incorporated in acrylic-based coatings for building envelope systems.

2. Experimental Methods

2.1. Materials and samples preparation

The TiO_2 rutile particles with labels <100 nm and <5000 nm size (diameter) were purchased from Sigma-Aldrich. TiO_2 rutile with 30, 50 and 500 nm particle sizes (diameter) were purchased from US Nano. All nanopowders used in this study were ≥ 99.9% trace metals basis and were employed as obtained without further purification. All the nanoparticles were co-pressed axially into a layered pellet at 28 MPa for 2 min to further study their band gap and reflectance properties.

The used colourant is a commercial black iron (II, III) oxide-based dispersion with a colour index PBk11 and 48% pigment content from Chromaflo. The technical data sheet of such colourant describe that it is water-based and free of alkylphenol ethoxylate (APE) with propylene glycol as a co-solvent. Also, it contains lower levels of volatile organic compounds [31]. The five sets of commercial TiO_2 nanoparticles were combined with the colourant to obtain different concentrations (1, 3, 5, 8, 12, 16 and 20% w/w) to study the influence of size and concentration on the NIR reflectance performance. All samples were mixed in a beaker at room temperature until a homogeneous mixture was obtained and applied with the aid of a spatula on 35×35×3 mm^3 acrylic substrates. The visual aspect of all samples is shown in Figure 1.

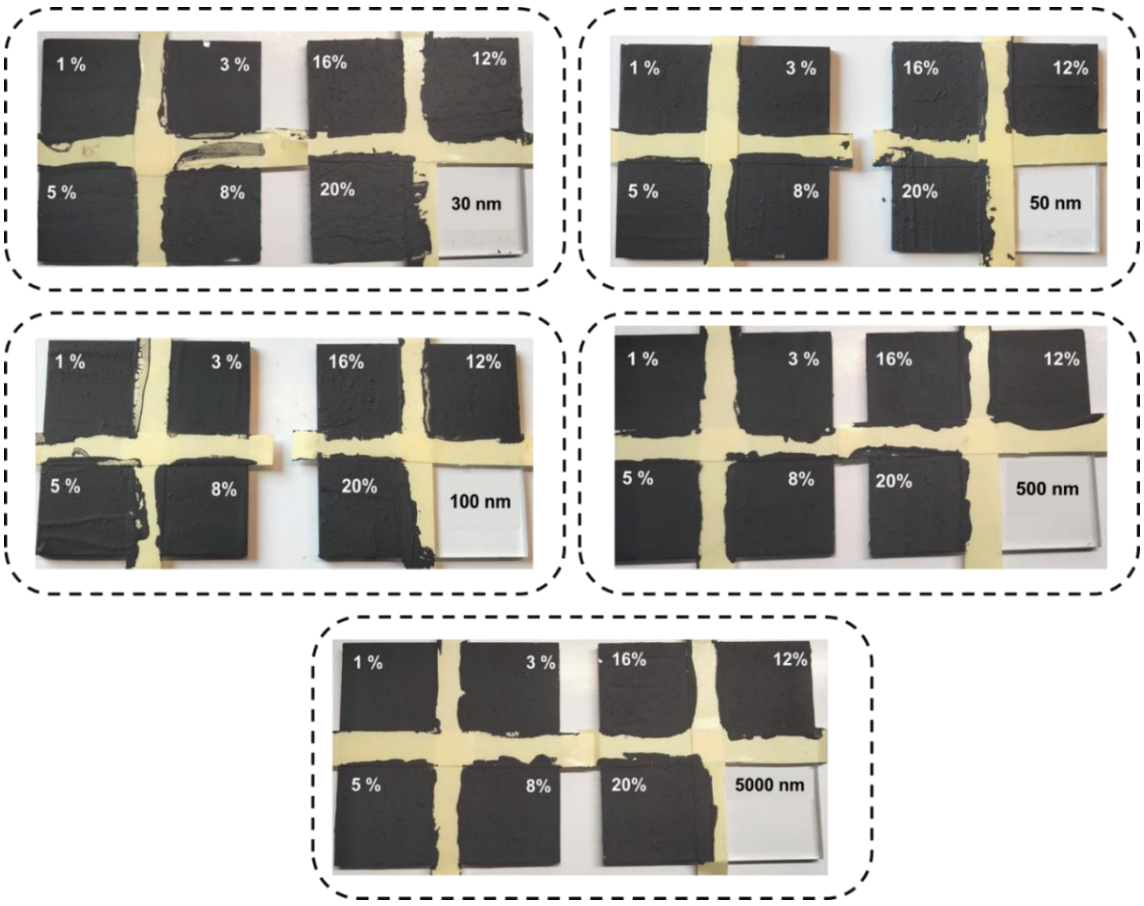

Figure 1: Photographs of the TiO_2-doped black colorant samples in acrylic substrates.

2.2. Characterization techniques and instrumentation

The morphologies and size distribution of the TiO_2 nanoparticles were observed in a High-Resolution Environmental Scanning Electron Microscope (SEM) with X-Ray Microanalysis and Electron Backscattered Diffraction (EBSD) analysis using an acceleration voltage of 25 kV (Quanta 400 FEG ESEM/ EDAX Genesis X4M). The SEM images were taken at 20000×, 50000×, 100000× and 200000× magnifications.

Structural characterization was performed by X-ray diffraction (Rigaku SmartLab; 45 kV and 200 mA) at room temperature using Cu-K_α radiation (1.540593 Å) and the Bragg–Brentano θ/2θ geometry in the 10°-90º 2θ range, with a step of 0.02° and scan rate of 12° min^{-1}. This system offers high-resolution data via a Johansson Ge $K_{\alpha 1}$ monochromator.

2.3. Reflectance and colourimetric assessment

To study the optical properties of a given material one needs to measure its reflectance spectrum as a function of wavelength. The spectral reflectance was obtained following the Standard Test Method for Solar Absorptance, Reflectance, and Transmittance of Materials Using Integrating Sphere – ASTM E903 [32]. The measurements were performed with a modular spectrophotometer (FLAME-T and FLAME-NIR Ocean Optics), equipped with a 30 mm integrating sphere Spectralon® coated with 8º angle port allowing determine the hemispherical (specular and diffuse) reflectance in the solar range 200 – 1650 nm. During the measurements, a Spectralon® disc was used for the collection of the baseline, in interval measurements of 5 nm, considering that the absolute accuracy should be less of 0.02 units or approximately 2%.

The spectral reflectance (SR, 200 – 1650 nm), Eq (1), and the short wave near-infrared radiation (SR_{nir}, 700 – 1650 nm), Eq (2), were calculated based on the 100 selected ordinates of Table X2.1 of ASTM E903 [32] and Air Mass of 1.5 of ASTM G173 [33]. Each sample was measured in three different points and the average is presented.

$$SR = \sum_{i=1}^{100} R\lambda/100 \qquad (1)$$

$$SR_{NIR} = \sum_{i=46}^{100} R\lambda/100 \qquad (2)$$

where R is the measured total reflectance by the spectrophotometer, and λ is the wavelength weight of Table X2.1.

Subsequently, the spectral irradiance was calculated considering the AM1.5 of the Sun at the Earth surface (Wm^{-2} nm^{-1}), according to the ASTM G197 [34] to a vertical surface. Since a large portion of the solar irradiance occurs in NIR range, at around 54.6%, it should be important to consider this region when optimizing the reflectance of these coatings. Therefore, the weighted reflectance (W_R) is calculated as follow:

$$\mathbf{W_R = 0.034SR_{UV} + 0.42SR_{Vis} + 0.546SR_{NIR}} \qquad (3)$$

The colour of all samples was evaluated by measuring the spectral reflectance with the same equipment. The CIE colourimetric coordinates, lightness L* (black–white), a* (green–red) and b* (blue–yellow), were used as recommended by the Commission Internationale de l'Eclairage (CIE) in the range of 200–1650 nm range using standard observed of 10º, D65 illumination and after calibration with a white standard (Spectralon®). The chroma (C*) parameter representing the saturation of the colour was calculated as [35]:

$$\mathbf{C^*_{ab}} = [(\boldsymbol{a^*})^{\mathbf{2}} + (\boldsymbol{b^*})^{\mathbf{2}}]^{\mathbf{1/2}}\ , \qquad (4)$$

while the hue angle (h) is calculated using:

$$h_{ab} = tan^{-1}\ (b^*/a^*)\ . \qquad (5)$$

The colour difference (ΔE) between two materials (1, 2) can be obtained using:

$$\Delta E^*_{ab} = [(\Delta L^*)^2 + (\Delta a^*)^2 + (\Delta b^*)^2]^{1/2}, \quad (6)$$

where $\Delta L^* = L_1^* - L_0^*$ is the difference in lightness (with $\Delta L^* > 0$ indicating a lighter material), $\Delta a^* = a_1^* - a_0^*$ is the difference in red and green (with $\Delta a^* > 0$ indicating redder tones) and $\Delta b^* = b_1^* - b_0^*$ is the difference in yellow (with $\Delta b^* > 0$ indicating yellower tones).

TiO_2 is a semiconductor and a photoactive material, with high solar to electrical energy conversion efficiency [36]. When solar radiation is reflected or absorbed, different types of electronic transitions may ensue, depending on the band arrangement of the material [37, 38]. Using the Tauc equation [39], it is possible to estimate the band gap based on the energy-dependent optical absorption coefficient model [40].

$$\boldsymbol{\alpha h\nu = A\ (h\nu - E_g)^n}, \qquad (7)$$

where $\boldsymbol{h}$ is the Planck's constant (J.s), A the absorption constant, α is the absorption coefficient, *v* the light frequency (s^{-1}) and E_g the band gap energy (eV). The *n* exponent is connected to the type of electronic transitions and takes the value 2 for indirect allowed,

3 for indirect forbidden, 1/2 for direct allowed or 3/2 for direct forbidden transitions. From the possible methods for determining the optical band gap, one of the most truthful considers the diffuse reflectance spectroscopy. As such, Kubelka and Munk [41] converted the measured reflectance to the corresponding absorption spectra and deduced the KM function:

$$\mathbf{F}\,(\boldsymbol{R}) = \frac{\boldsymbol{\alpha}}{\boldsymbol{s}} = \frac{(\mathbf{1}-\boldsymbol{R}_{\infty})^{2}}{\mathbf{2}\boldsymbol{R}_{\infty}}, \qquad (8)$$

where s is the effective scattering coefficient and R_∞ the reflectance at an infinite thickness. Replacing F(R) in Eq. (1) results in:

$$[\mathbf{F}(\boldsymbol{R}_{\infty}).\mathbf{h\nu}]^{\frac{\mathbf{1}}{\boldsymbol{n}}} = \mathbf{A}\left(\mathbf{h\nu} - \mathbf{E_g}\right). \quad (9)$$

The optical band gap energy of the nanoparticles were calculated in three steps considering the methodology developed by Sangiorgi et al. [38] as shown in the flowchart presented in Figure 2.

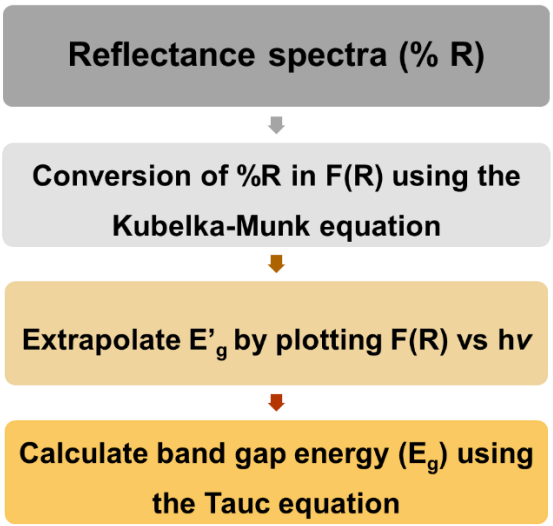

Figure 2: Methodology for the determination of optical band gap and electronic transitions. Adapted from Ref. [38].

3. Results and Discussion

3.1. Structural and morphological analysis of TiO_2 nanoparticles

The SEM images of TiO_2 nanoparticles are shown in Figure 3. These images show that the 30 nm, 50 nm and <100 nm nanoparticles present cubic and homogeneous morphology [Figure 3(a)- (c)]. It is also observed that, for the 500 nm size, the nanoparticles present a spherical morphology [Figure 3(d)] while the 5 µm nanoparticles [Figure 3(e)] have an irregular and heterogeneous morphology and a large distribution.

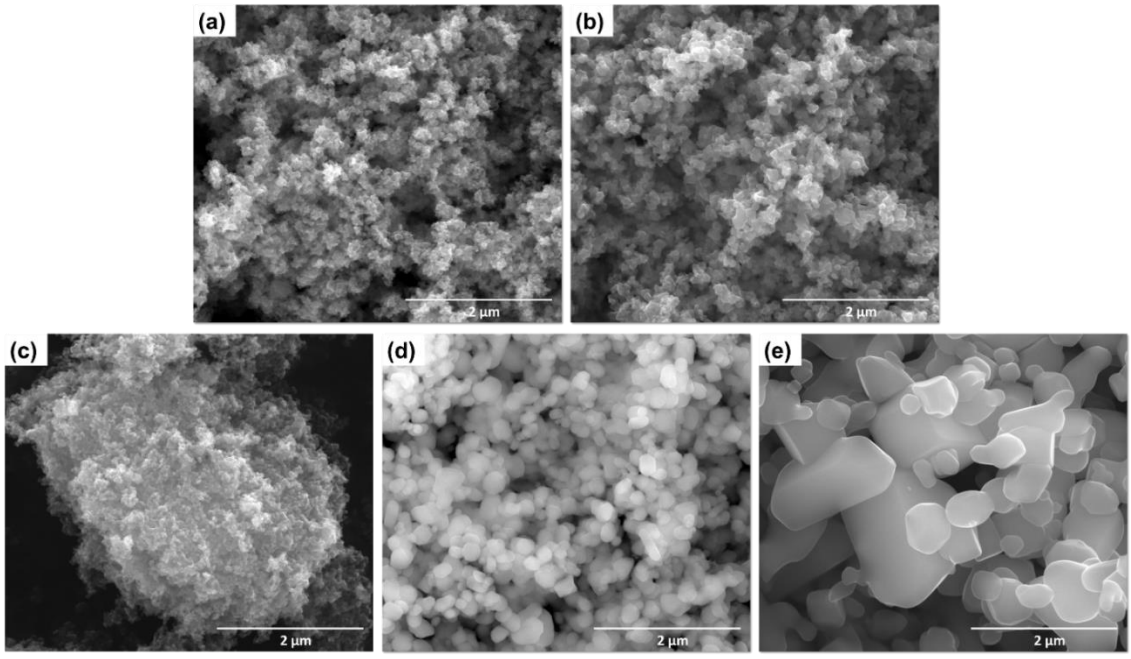

Figure 3: Scanning electron microscopy images of TiO_2 nanoparticles (a) 30 nm, (b) 50 nm, (c) <100 nm, (d) 500 nm and (e) <5000 nm. Scale bar: 2µm.

A size distribution analysis of the nanoparticles was carried out since commercial powders are usually characterized by a range of particle sizes. Thus, the particles are analysed by direct microscopy observation and the size is determined by frequency counts. As such, the sizes of the nanoparticles are characterized by the width of the Gaussian size distribution, as showed in Figure 4 (b). The obtained mean diameter (ø), standard deviation (σ), modus (dm) and median (d50%) are represented in Table 1.

Table 1: Size distribution statistics.

TiO_2	**ø (nm)**	**σ (nm)**	**d_m (nm)**	**$d_{50\%}$ (nm)**

30 nm	32.9	9.8	37.6	30.7
50 nm	50.0	22.5	42.4	47.1
< 100 nm	29.0	5.7	32.6	26.8
500 nm	158.5	7.5	150.2	147.5
< 5000 nm	1733.8	134.0	2274.2	1599.2

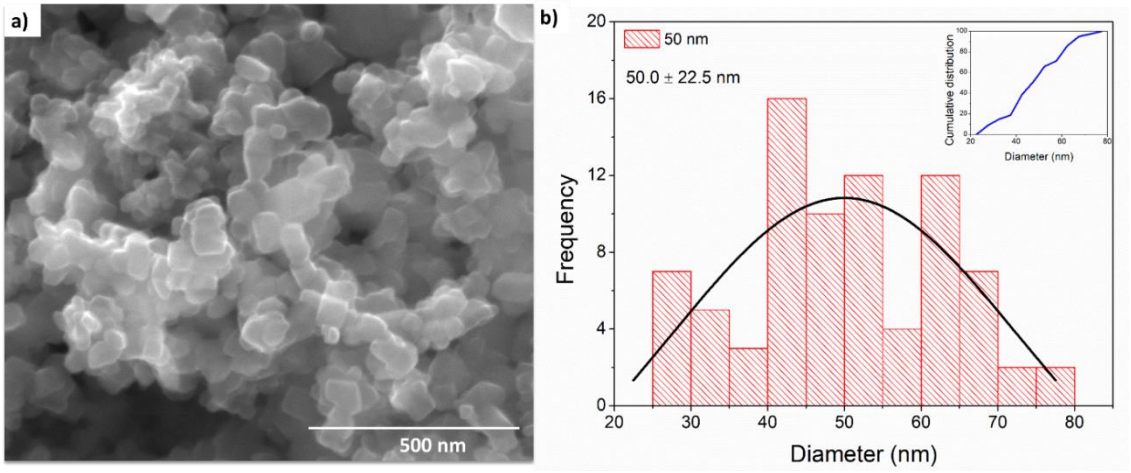

Figure 4: (a) Direct SEM observation measure for TiO_2 50 nm size nanoparticle and (b) Gaussian size distribution analysis (cumulative fractions as an inset).

The X-ray diffraction (XRD) patterns of the commercial TiO_2 nanoparticles are presented in Figure 5. The sharp and strong peaks observed in the diffraction patterns expose the crystalline nature of the powders and the presence of the characteristic reflections of rutile and anatase TiO_2 phases. All compounds crystallize in a tetragonal structure with a space group $P4^2/mnm$ for the rutile phase and $I4_1/amd$ for the anatase phase. The average crystallite size of the particles (D_{XRD}) was calculated using the Williamson–Hall relationship [42, 43]:

$$\boldsymbol{\beta_{total} = \beta_{size} + \beta_{strain} = \frac{k\lambda}{D_{XRD}\cos\theta} + 4\eta \tan\theta}\ , \quad (10)$$

where k the Scherrer constant (~ 0.94 for spherical NPs), λ the incident X-ray wavelength, β_{total} is the full width at half-maximum of the XRD peak, θ the diffraction angle and η the microstrain parameter. Figure 5(b) shows a plot of $\boldsymbol{\beta_{total}\cos\theta\ /k\lambda}$ versus $\boldsymbol{4\sin\theta\ /k\lambda}$ for all samples, allowing the estimation of η and D_{XRD} (Table 2). The values obtained for

D_{XRD} are in good agreement with the ones measured by SEM. Internal strain can be considered insignificant [$\eta < 0.2\%$] and therefore does not have a significant role in the key physical properties of these nanomaterials.

Table 2: Diameters of the commercial TiO_2 nanoparticles obtained from SEM and XRD analysis. Calculated microstrain and phase percentages are also shown.

TiO_2	D_{SEM} (nm)	D_{XRD} (nm)	Strain by XRD	Rutile / Anatase
30 nm	32.9 ± 9.8	26 ± 3	(11 ± 3) $\times 10^{-4}$	100% / 0%
50 nm	50.0 ± 22.5	50 ± 8	(13 ± 2) $\times 10^{-4}$	100% / 0%
< 100 nm	29.0 ± 5.7	33 ± 4	(9 ± 3) $\times 10^{-4}$	100% / 0%
500 nm	158.5 ± 7.5	194±39	(150 ± 9) $\times 10^{-5}$	99.6% / 0.4%
< 5000 nm	1733.8± 134.0	NA	NA	95% / 5%

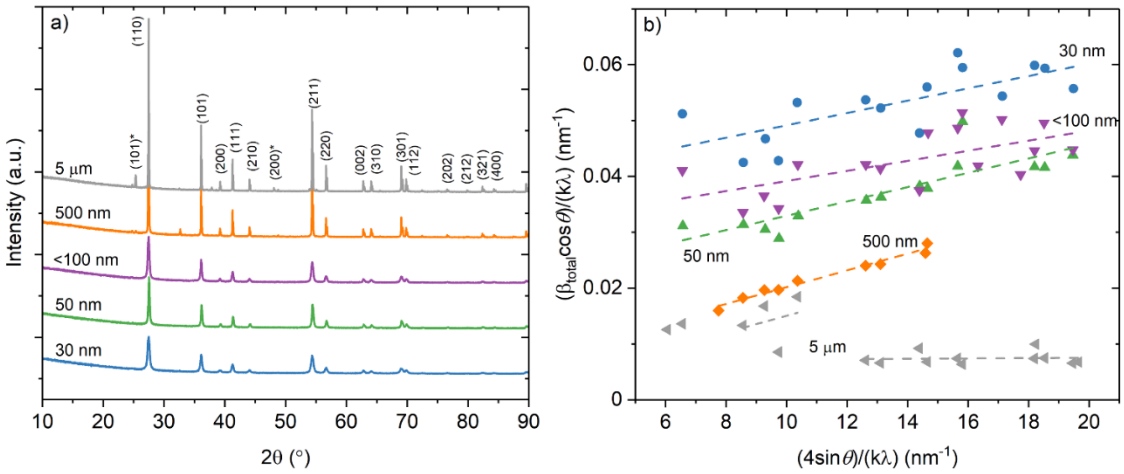

Figure 5: (a) XRD patterns of commercial rutile and (*) anatase TiO_2 nanoparticles with different diameters and (b) linear fit using the Williamson–Hall correlation (the different slopes represent different mean strains and the line interception gives the inverse particle size).

To accurately assess the thickness of the painted layers, a SEM analysis was performed. The sample was treated with liquid nitrogen to fracture at low temperature without changing the integrity of the coating. With a carbon adhesive, the fractured coating was rescued. The SEM results revealed a coating thickness of 150 µm (Figure 6). A 3D profilometer map analysis was also performed and a nominal peak-to-peak surface

roughness of ~11 µm was obtained for the acrylic substrate [Figure 7(a)] and of ~15 µm for the coating on top of the acrylic [Figure 7(b)].

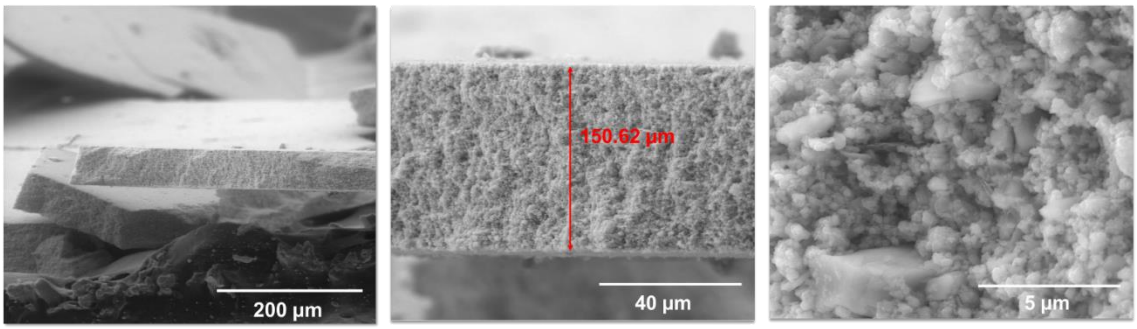

Figure 6: Measured thickness of the painted layer of the conventional colourant by electron microscopy.

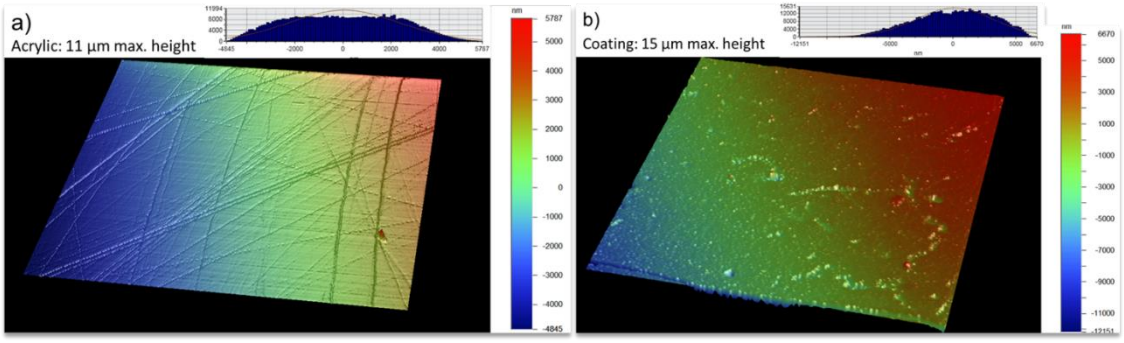

Figure 7: 3D profilometer maps for the (a) painted layer of conventional coating and (b) acrylic substrate (1mm × 1mm area) allowing the determination of the surface roughness (σ) of the samples.

3.2. Optical band gap and electronic transitions determination

The optical bandgap energy indicates the capacity of a material to absorb or reflect light. According to the method described by Sangiorgi et al. [38], the first step is the analysis of the reflectance and absorbance of the material. A typical reflectance spectrum for each nanoparticle pellet is reported in Figure 8(a). The spectrum present analogous trends with all the nanoparticles absorbing in the UV region and reflecting most of the light in the visible region. For example, for λ= 420 nm most of the radiation is reflected (from 77% to 95%), a typical behaviour for TiO2 materials [44]. TiO_2 can absorb or

scatter UV light and reflects most of the visible light, so that its whitish colour arises from light diffusion processes when particles are closely packed. On the other hand, for λ= 260 nm, the reflectance is very low due to electron/hole generation since incident photons have sufficient energy and the material absorbs the radiation. The reflectance spectra were converted in a F(R) representation using the Kubelka-Munk equation [Equation (9)].

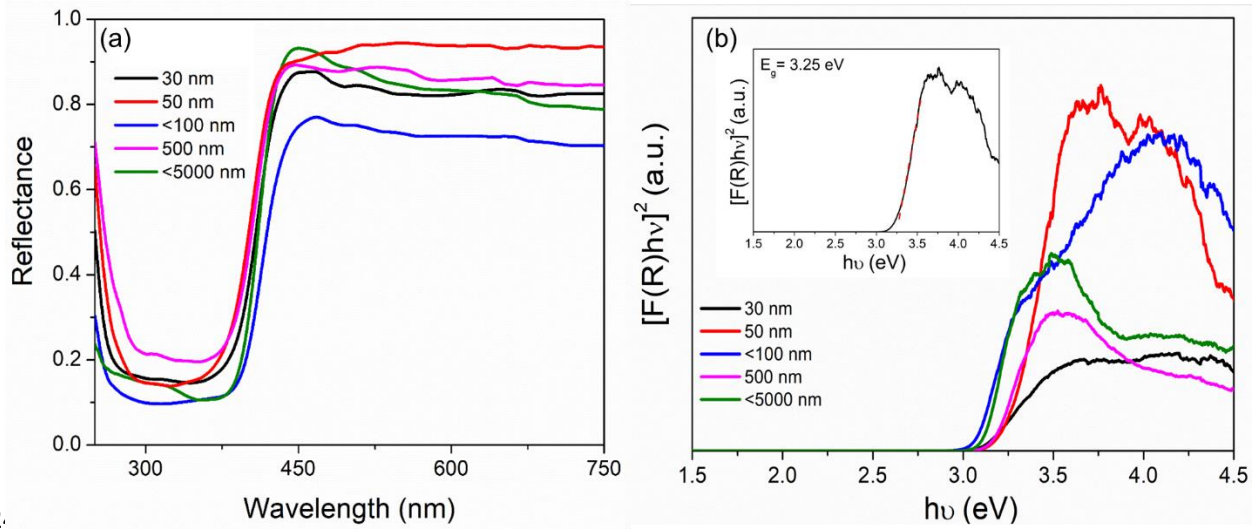

Figure 8: (a) Reflectance spectrum of the nanoparticle pellets and (b) Graphical representation of $[F(R)\ h\nu]^2$ versus hν. The determination of Eg for the 50 nm TiO_2 is shown in the inset.

For polycrystalline materials, as our TiO_2 nanoparticles, the density of states is non-zero inside the gap, with band tails induced by disorders, mainly produced by impurities or structural disorders [45]. Band tail states are electronic states present above the valence band or below the conduction band that not only narrow the band gap, but also constrain the recombination of electrons by localizing photo-induced holes [45, 46]. For these reasons, the usual method to determine the optical band gap is to use the Tauc equation [Equation 3]. In a shortened way, E_g can be assessed from the plot obtained from the lowest conduction band and highest valence band edge. For the calculation of the optical band gap E_g, the determination of the correct value of the *n* exponent is critical. In that regard, it is well established in the literature that anatase TiO_2 is an indirect band gap semiconductor while rutile TiO_2 has a direct band gap (for which *n* =1/2) [47, 48].

Therefore, we determined the optical band gap energy E_g by fitting the linear section of the $[F(R)h\nu]^{1/n}$ versus (hν) plot and extrapolating to F(R)hν=0, where the real absorption coefficient for those energies is still non-zero due to the band tails [Figure 8(b)]. Values between 3.06 and 3.25 eV are obtained (Table 3), close to those found in the literature (~ 3.0 eV for TiO_2 rutile) [49-51]. The slight differences between these values are attributed to the particle size of the TiO_2 nanoparticles and to their crystalline phase, since the 500 nm and <5000 nm nanoparticles are composed by 0.4% and 5% of anatase phase, respectively. These small amounts may be sufficient to influence the overall band gap energy.

Table 3: Experimental band-gap energy and total reflectance values obtained for the TiO_2 nanoparticles used.

Method	**Nanoparticles**				
	30 nm	50 nm	<100 nm	500 nm	<5000 nm
R_{Total}	0.775	0.923	0.642	0.949	0.800
E_g (eV)	3.10	3.25	3.06	3.15	3.10

Under similar conditions, higher optical band gap energies lead to a reduction of the intrinsic absorption region and thus to an enhancement of the reflection [52]. TiO_2 particle size is an important parameter to be taken into consideration since it affects the spectral properties when their size becomes comparable with the size of the exciton [53]. When their size reduces from the bulk to the first excitation state (Bohr radius), the size quantization effect appears, owing to the spatial confinement of charge carriers [54]. Their reduction results in a size increase of the conduction band and decrease of the valence band, resulting in a band shift that influences the optical properties [55]. Several works reported that particles with diameters in the 5.5-200 nm range display distinct size quantization effect leading to a blueshift between 0.067 to 0.6 eV [56-58].

Figure 9 shows the reflectance of the nanoparticles as a function of the band gap energy calculated. One can observe that the <100 nm size nanoparticle that has a lower band gap amongst the nanoparticles studied, shows lower reflectance which will influence the functional properties of composite paint. Following this statement, one can already predict that the 50 nm and 500 nm nanoparticles will present the best overall effect in the reflectance of the colourant since it has the largest calculated optical band gap (3.25 and 3.15 eV) and the highest reflectance values (0.92-0.95).

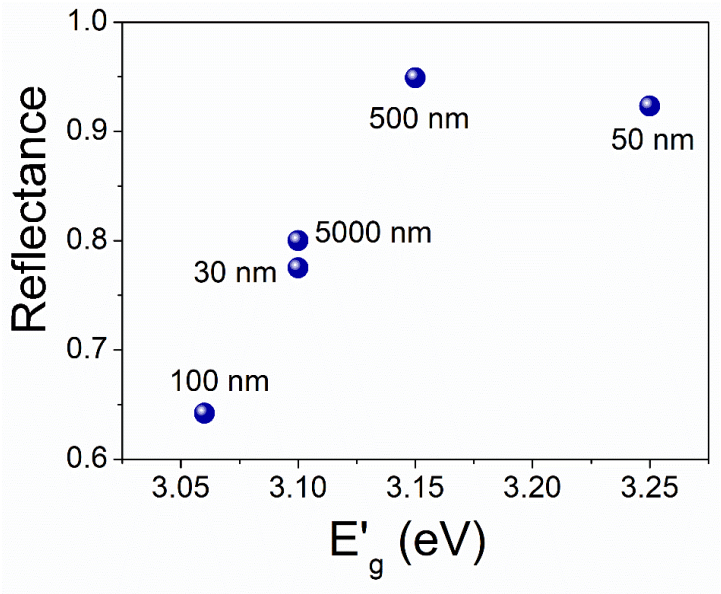

Figure 9: Reflectance as a function of band gap energy of the TiO_2 nanoparticles.

3.3. Effect of TiO_2 doping on the optical properties of a conventional black colourant

The spectral reflectance is the most critical parameter when evaluating the performance of solar systems, including passive buildings. To measure such reflectance, the ASTM E903 method procedure was chosen, which allows to evaluate the NIR-reflectance behaviour [32]. Typical spectral reflectance spectra for the colourant doped with TiO_2 nanoparticles is shown in Figure 10.

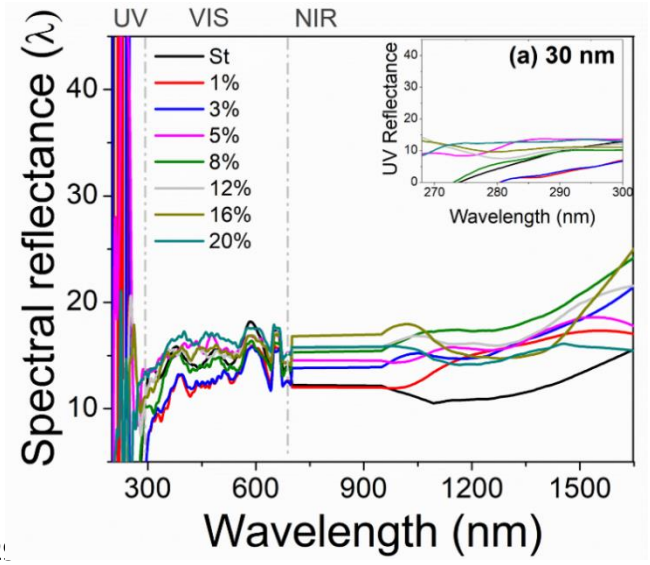
UV
VIS
NIR
Spectral reflectance (λ)
Wavelength (nm)
St
1%
3%
5%
8%
12%
16%
20%
(a) 30 nm
UV Reflectance
Wavelength (nm)

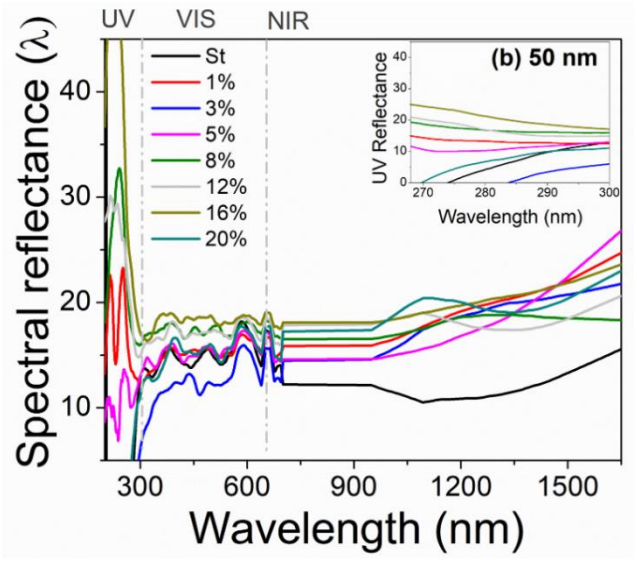
UV
VIS
NIR
Spectral reflectance (λ)
Wavelength (nm)
St
1%
3%
5%
8%
12%
16%
20%
(b) 50 nm
UV Reflectance
Wavelength (nm)

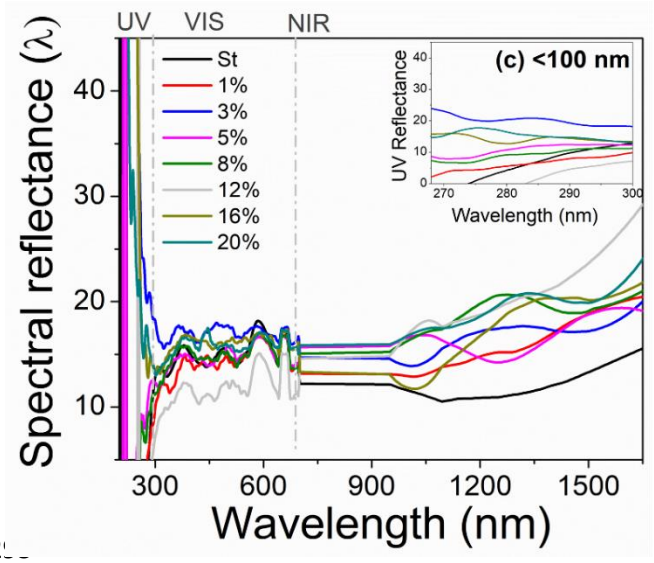
UV
VIS
NIR
Spectral reflectance (λ)
Wavelength (nm)
St
1%
3%
5%
8%
12%
16%
20%
(c) <100 nm
UV Reflectance
Wavelength (nm)

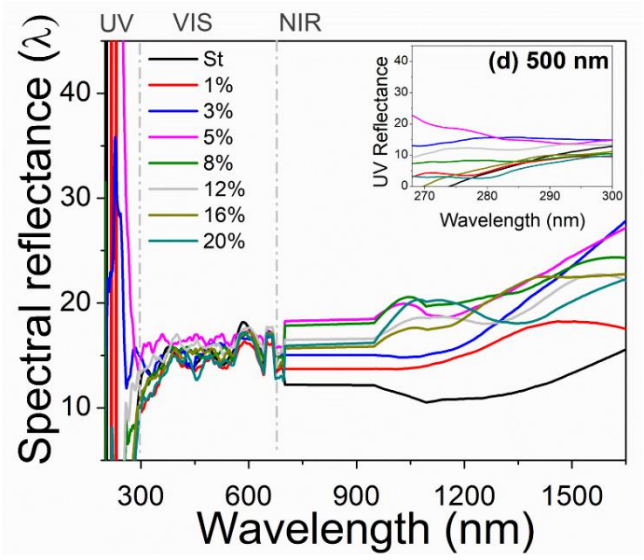
UV
VIS
NIR
Spectral reflectance (λ)
Wavelength (nm)
St
1%
3%
5%
8%
12%
16%
20%
(d) 500 nm
UV Reflectance
Wavelength (nm)

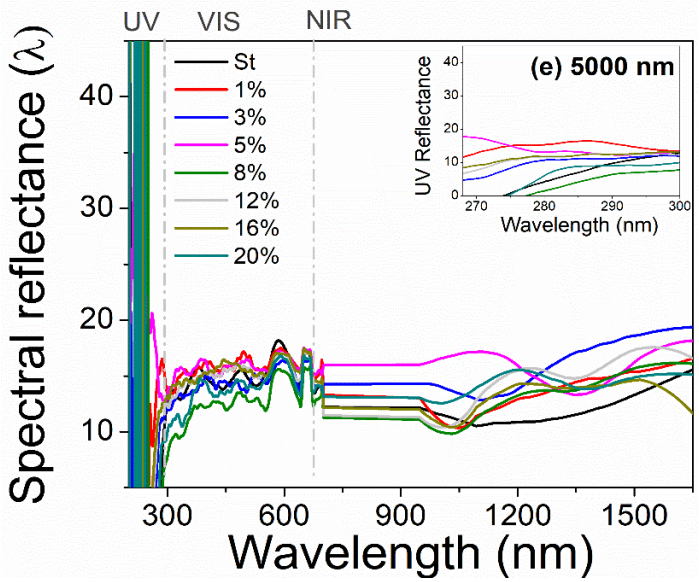

Figure 10: Spectral reflectance behaviour of the TiO_2-doped black colorant with (a) 30 nm, (b) 50 nm, (c) <100 nm, (d) 500 nm and (e) <5000 nm (inset: UV performance of the nanoparticles studied).

From these results, we observe that all the doped samples present a similar performance (as expected) by partially absorbing visible light since we are dealing with black coatings. With a high refractive index (n=2.72), TiO_2 strongly absorbs in the UV region and effectively scatters light [59]. Similarly, almost all the TiO_2-doped colourant samples present the same strong absorption pattern in the UV region, especially for low doping concentration (between 1 and 5%). After exceeding such concentrations, the behaviour in the UV region is not linear. This phenomenon may be due to the agglomeration of the nanoparticles at higher concentration. In fact, an important drawback is created by the strong tendency of NPs to agglomerate due to their large specific area [60]. TiO_2 particles are prone to aggregate in slurries so that it is necessary to stabilize the nanoparticles in the coating formulation against settling and flocculation. Typically, several surface dispersing agents are used to disaggregate nanoparticles, although they typically also lead to a loss of gloss or brightness and are incapable of maintaining a significant degree of spacing between the TiO_2 particles to enhance the

light scattering of the dispersed TiO_2 [61-63].

As for the near-infrared region, the samples present noteworthy differences with an enhanced NIR reflectance when compared to the conventional colourant. For better comparison, the calculated total (Table 4) and near-infrared reflectance are presented versus the TiO_2 concentration for the different diameters (Figure 11). While the conventional black colourant absorbs most of the NIR radiation, with a reflectance value of 0.112±0.016, the doped samples show a significant enhancement for the near-infrared region, with reflectance values from 0.120 to 0.208 (an up to 86% increase).

Table 4: Calculated average total solar reflectance of the TiO_2-doped samples.

Concentration (w/w)	**Total Solar Reflectance**				
	30 nm	50 nm	100 nm	500 nm	5000 nm
Standard			0.130±0.016		
1%	0.124±0.007	0.169±0.008	0.144±0.013	0.144±0.011	0.117±0.069
3%	0.133±0.009	0.174±0.025	0.164±0.026	0.168±0.008	0.150±0.011
5%	0.143±0.021	0.165±0.018	0.151±0.009	0.186±0.012	0.163±0.006
8%	0.155±0.011	0.178±0.004	0.153±0.009	0.171±0.013	0.150±0.010
12%	0.162±0.013	0.179±0.008	0.151±0.018	0.170±0.013	0.148±0.003
16%	0.163±0.007	0.197±0.009	0.168±0.010	0.160±0.009	0.144±0.011
20%	0.159±0.008	0.162±0.023	0.172±0.003	0.138±0.033	0.136±0.005

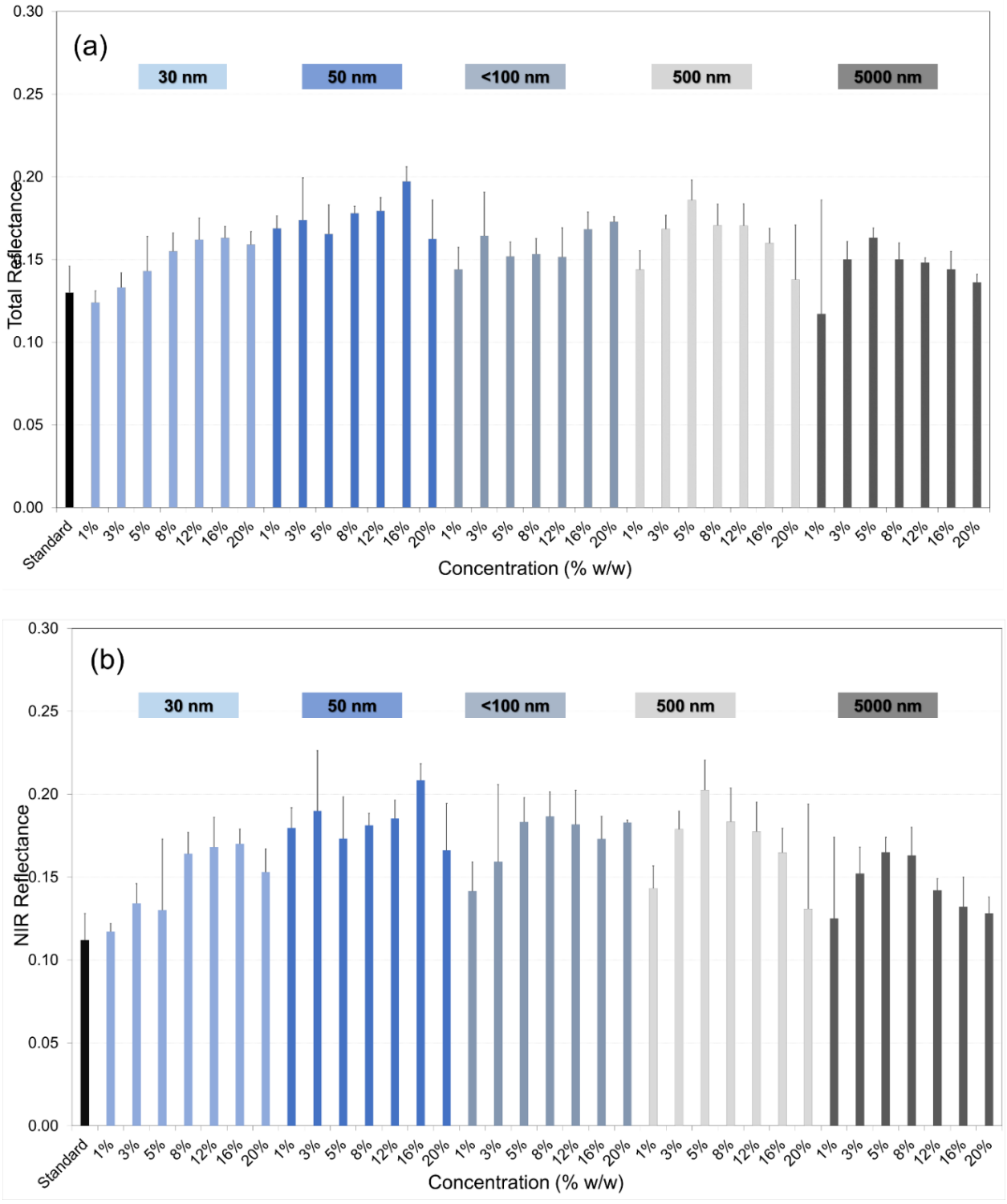

Figure 11: Calculated (a) total average and (b) NIR reflectance using ASTM E903 of the TiO_2-doped black colourant samples.

From Figure 11(a), one can see that the total reflectance typically increases with the concentration, reaching a maximum for a concentration of approximately 12-16% for

smaller particles and 5-8% for larger ones. The behavior is similar for the NIR reflectance [Figure 11(b)], with a decay of the reflectance for high concentrations (16-20%). It is known that TiO_2 particles scatter about 75% of light through diffraction, consequently increasing its effective scattering volume [64]. However, an undesirable consequence of the large scattering volume of TiO_2 particles is that, as the inter-particle distance decreases with increasing concentration, pigment crowding effect occurs at relatively low particle concentration, inducing a decay of the total light scattering [64-66]. In fact, if two or more particles are in actual contact with each other or if they are closer together than the ideal spacing distance, the particles behave as a large aggregate resulting in reduced light scattering [61]. As such, the scattering coefficient is only linear at very low concentrations (Beer's law region), being below the linear value for higher concentrations [65, 67]. Furthermore, according to Auger et al. [68] the phenomenon, in which the scattering depends on the closeness of the particles, is a specific manifestation of multiple scattering that is known to occur in white paints pigmented with TiO_2 rutile particles [69]. Therefore, the solar reflectance reduction above a certain particle concentration is a consequence of the increase of the number of particles that leads to a decrease in the total scattering.

To design an optimal nanoparticle-doped coating, that maintains the reflectances on the visible region but enhances the NIR reflectance, Baneshi et al. [70] proposed calculating the reflectivity of the NIR (ρ_{NIR}) and VIS (ρ_{VIS}) regions weighted by the human eye perception as:

$$\rho_{VIS} = \frac{\int_{0.38}^{0.78} \rho(\lambda)\eta(\lambda)\mathrm{I}(\lambda)d(\lambda)}{\int_{0.38}^{0.78} \mathrm{I}\,(\lambda)d(\lambda)}, \quad (11)$$

and

$$\rho_{NIR} = \frac{\int_{0.78}^{2.6} \rho(\lambda)\eta(\lambda)\mathrm{I}(\lambda)d(\lambda)}{\int_{0.78}^{2.6} \mathrm{I}\,(\lambda)d(\lambda)}\ . \quad (12)$$

where I(λ) is the solar irradiation, η(λ) is the standard brightness and ρ(λ) is the spectral reflectivity of the coating. In this optimization principle, one has to consider the nanoparticle composition and size, in addition to the density of the nanoparticles [4]. Taking this into consideration, an optimum reflectance coating, without affecting its aesthetic properties, is achieved by optimizing the ratio (R) between the NIR and VIS reflectance:

$$R = \frac{\rho_{NIR}}{\rho_{VIS}} \qquad (13)$$

The calculated R values are presented in Table 5, showing that the optimized value is reached for the 50 nm size nanoparticles (R~1.09), while the minimum value was found for <5000 nm (R~ 0.909).

Table 5: Parameter R for the different studied nanoparticles.

TiO_2 nanoparticle	**R**
30 nm	0.990
50 nm	1.093
< 100 nm	1.051
500 nm	1.082
< 5000 nm	0.909

When trying to improve the reflectance one must consider the source of the incident irradiance. For terrestrial applications, the irradiance source is the terrestrial solar spectral irradiance at normal incidence air mass 1.5 (AM 1.5). Here, spectral irradiance distribution was calculated using the ASTM G197 [34] for vertical surfaces, integrated over the solar spectrum. This standard test method separates the contributions from direct and diffuse radiation, allowing more exact calculations of diffuse heat gains [71]. The resulting spectra for the TiO_2-doped samples are presented in Figure 12.

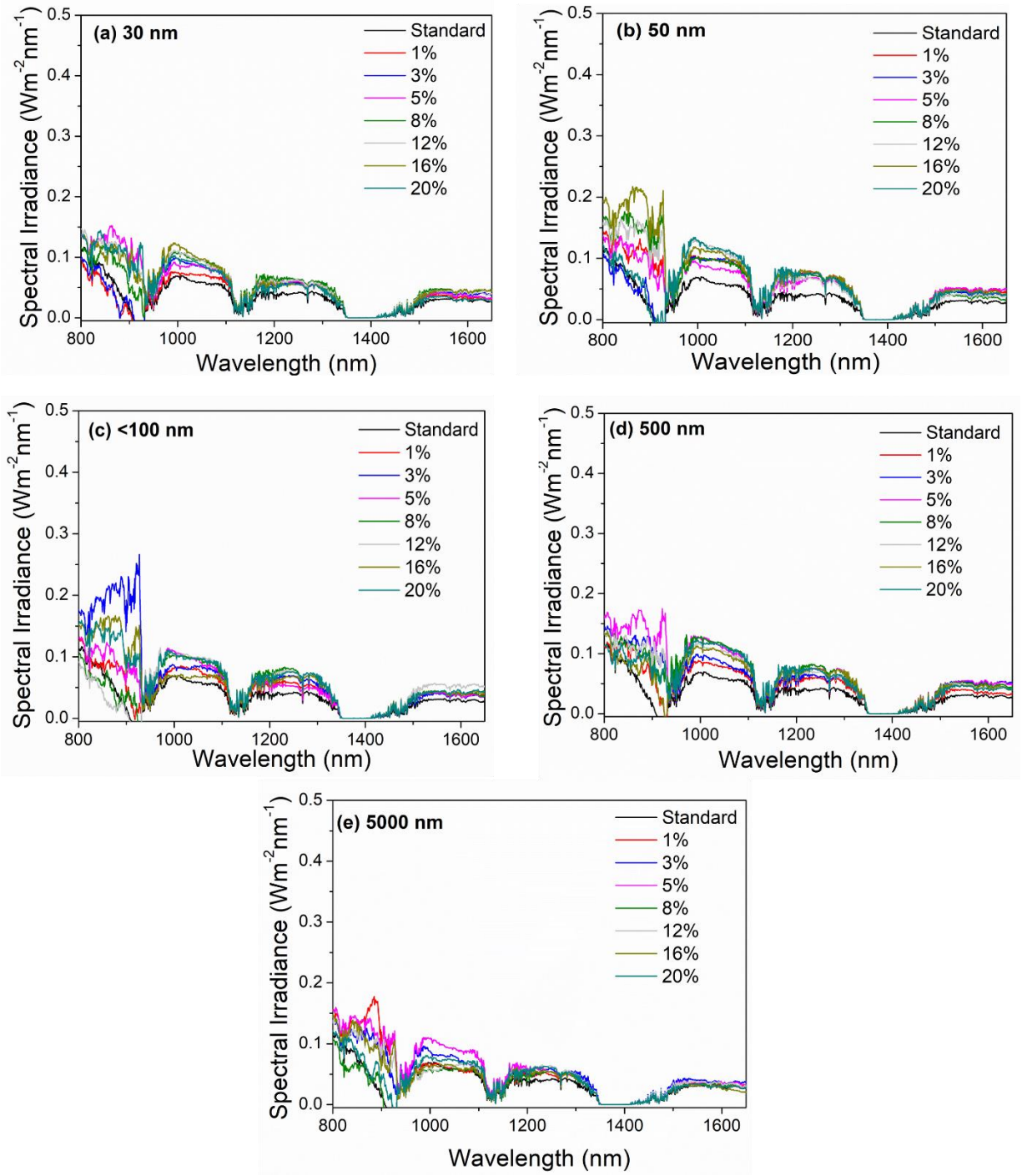

Figure 12: Near-infrared solar spectral irradiance (W $m^{-2}nm^{-1}$) distribution for the TiO_2-doped black samples with (a) 30 nm, (b) 50 nm, (c) <100 nm, (d) 500 nm and (e) <5000 nm using ASTM G197.

As an example, Figure 13 shows the weighted reflectance, calculated using Equation (3), for TiO_2 50 nm particle size doped samples to understand how the reflectivity is distributed. We clearly observe that the infrared reflectance was improved

for all tested mixtures with a maximum of 0.112 reflectance reached for the 16% concentration (w/w), when compared to the conventional black colourant value which is of only 0.052. All samples present the same behaviour in the UV region, but in the visible region, the reflectance is also affected, with all samples presenting a slight enhancement.

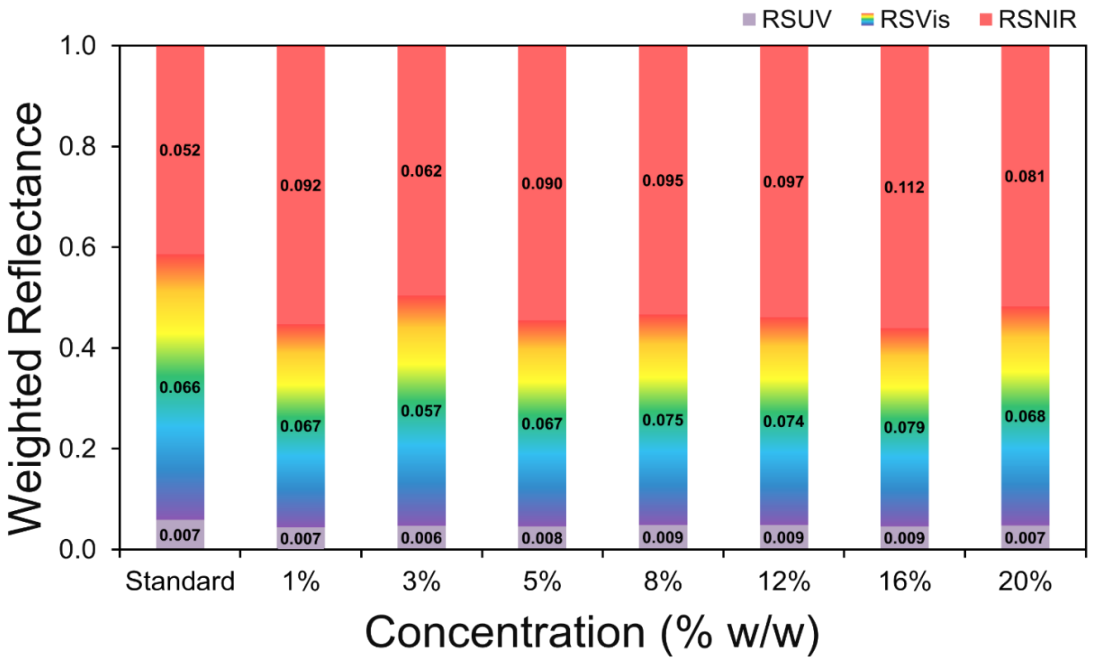

Figure 13: Weighted reflectance calculation of 50 nm size TiO_2-doped black colourant.

Since we are using a dark colourant, the VIS and IR region reflectance are expected to be lower than in other cool colourants. However, the results clearly demonstrate that the incorporation of nanoparticles in the conventional black colourant increases the reflectance of the samples, with maximum values typically in the 5-16% concentration range. Although all samples present higher NIR and total reflectance than the black colourant, a global maximum was observed for a TiO_2 rutile with 50 nm size (with a 0.20 reflectance compared to 0.13 for the standard colourant) for 16% concentration. Concerning the <100 nm size nanoparticles, it is clear that the total reflectance values are lower than the other doped samples. This is mainly due to the large size distribution (Table 2) and the

smaller optical band gap energy of the nanoparticles (2.98 eV), the lowest amongst the nanoparticles used in this study.

3.4. Colourimetric assessment

As mentioned, black colourants are commonly used mainly for aesthetic purposes. Therefore, the colourimetric assessment becomes a crucial factor to consider when formulating new NIR-reflective coatings. One of the aims of this study was to improve the reflectance of the coating (which consequently will increase its thermal performance) without excessively changing its colour. Figure 14 presents the CIELab coordinates for all doped samples, including the conventional black colourant (standard in black dot). The (x-y) axis represent the variation between green (-a*) and red (+a*), and between yellow (+b*) and blue (-b*), respectively. The lightness (L*) ranges vary from 0-100 (white to black). In addition to the sample coordinates, the rectangles represent the variation in RGB colour for the axis limits in the CIELab system a*b* (-5.0 – 5.0) and L* (39 – 47).

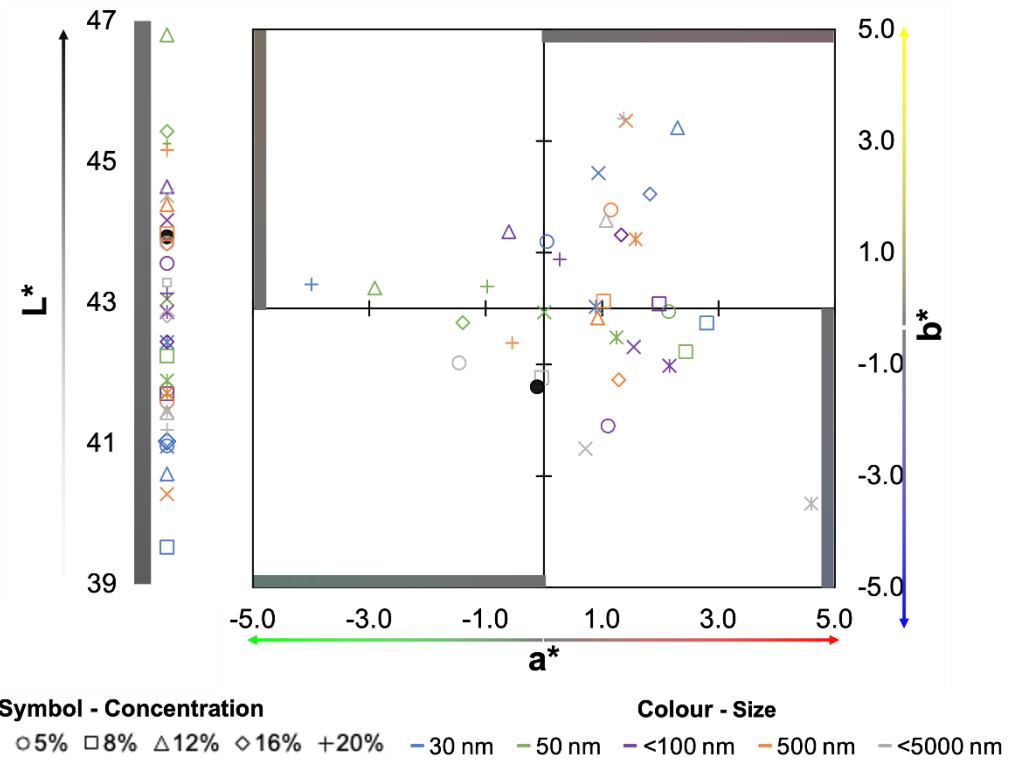

Figure 14: CIELab coordinates for all samples. The black dot represents the conventional black colourant (standard).

The conventional black colourant (standard) is described as a dark grey colour with a bluish to yellowish undertones pigment. In this study, we confirmed that the standard sample presents a blueish tone (b* is negative, and a* is almost zero). However, the lightness value should be lower than 40 to be considered a dark colour [72, 73]. Here we found that the black colourant (L*=43.933) could be classified as a light grey [74, 75].

The achromatic colours are shades of white, grey, and black, for which the reflection in the visible range is similar in all wavelengths. As verified in the spectral reflectance (Figure 10), the samples present an achromatic aspect. In other words, in the a*-b* coordinates (Figure 14), the colour turns matte and achromatic similar to the origin [76] with the lower difference between the coordinate a* and b* [77]. As described by Piri et al. [78], the chroma is strongly affected by the particle size, the particle absorption coefficient and the real part of the refractive index. The higher chroma variation was found for <5000 nm and 3% concentration (w/w), and the lower for the 50 nm nanoparticles and 16% concentration in the colorant. This result is in accordance with the study conducted by Piri et al. [79] where, for stronger absorbing particles, the increment in the diameter will lead to higher chroma values. As seen in Figure 14, the (5000 nm, 3%) and (30 nm, 20%) doped samples can be considered chromatic with a significative difference in chroma considering the other doped samples.

The minimum colour difference noticeable by the human eye is typically considered as $\Delta E=1$, but a limit value of 3 is typically considered, following the statement by Cozza et al. [80] and Mokrzycki et al. [81]. In Figure 15(a) we represent the combined effect of the doping concentration and nanoparticle size. Looking closer to the results, the sample with <5000 nm doped at 8% had the lowest ΔE value (0.67), while the 500 nm

with 1% sample presented the highest value (15.13). Almost 50% of the samples had a colour difference higher than 3. This effect was expected due to the introduction of a white particle (TiO_2) in the black colorant. The colour difference is strongly affected by the lightness, as the chroma (a-b) parameter is not so different between the samples.

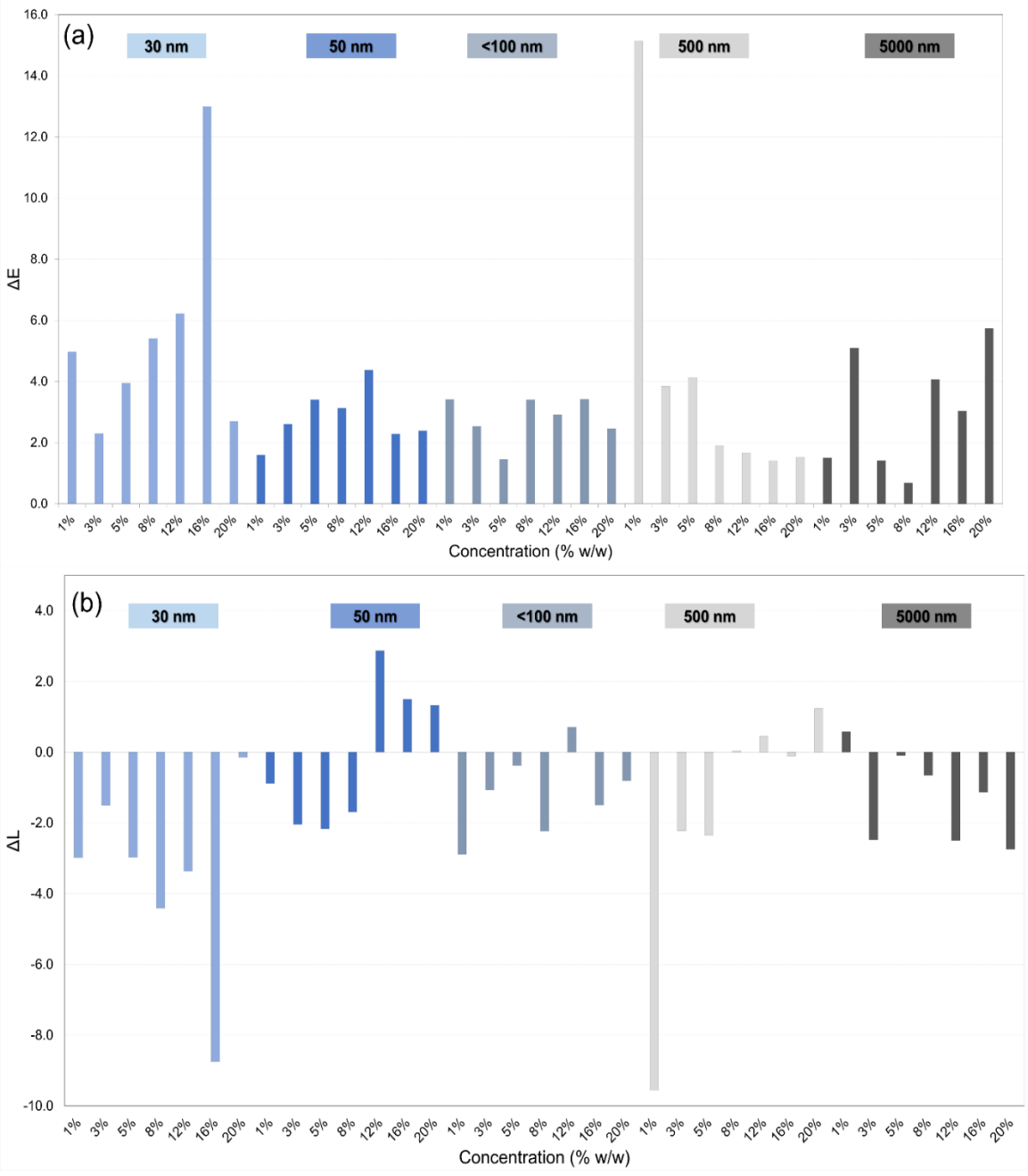

Figure 15: (a) Colour and (b) lightness difference of TiO_2-doped black samples with the nanoparticles used in the study when compared with the conventional colorant.

The lightness difference is given in Figure 15(b). The samples with lower ΔL also have the lowest ΔE [see Figure 15(a)]. The incorporation of TiO_2, against expectations, turned almost all samples darker than the standard colourant. Note also that the sample with 30 nm size and with 8% concentration has a medium tone lightness classification, unlikely to the standard, and all the other samples that are classified as a light-medium tone. The lightness variation is also in agreement with the study carried out by Piri et al. [78, 79], where the increase in the diameter leads to higher lightness values. Such performance can be explained by the intrinsic properties of the particles, as materials with larger extinction coefficients will lower the visible reflectance and consequently decrease the lightness [82].

4. Conclusions

There is an increasing tendency in applying darker colours in envelope systems, while trying to reduce the effect of solar radiation, which proves the relevance of including high-reflective nanoparticles in black colorants for coatings. Here, we studied how the reflectance and colorimetry of a conventional black colorant vary depending on the properties (size, concentration) of incorporated TiO_2 nanoparticles.

The spectral reflectance results demonstrated that the incorporation of nanoparticles in the conventional black colorant increases the reflectance of the samples. The most adequate TiO_2 composition for enhancing the reflectance is the 50 nm nanoparticles with 16% doping concentration, with a 0.20 total reflectance when compared to only 0.13 for the standard colorant. Regarding the colour assessment, it was found that the incorporation of TiO_2 nanoparticles affects the perception of lightness and colour, which was expected since a white pigment was introduced in the composition, turning most of the samples darker (decrease in the value of the coordinate L*) than the standard colorant, whereas only 8 samples were found to have the reverse effect. For the

50 nm samples, enhancing the concentration leads to a reduction of the lightness. Nevertheless, a linear correlation between the concentration and the lightness parameter was not observed.

To make a balance between the colour difference and the experimental results obtained for the optical band gap calculation of the TiO_2 pellets and optimization parameter R, the reflectance results of the doped colorant validate that the best nanoparticle to be used is the TiO_2 with 50 nm size. Such nanoparticles result in a ΔE below 3 for the concentrations between 1-3% and 16%-20%, which makes them suitable candidates to be used as dopants without significantly affecting the colour.

Credit authorship contribution statement

Conceptualization: R.C.V., N.M.M.R., J.V.; **Methodology**: R.C.V., C.D. and A.S.; **Formal Analysis**: R.C.V., C.D. and A.S; **Investigation:** R.C.V and J.V.; **Data Curation**: R.C.V, C.D and A.S.; **Validation:** N.M.M.R. and J.V; **Writing- Original Draft and Review**: R.C.V, C.D, A.S, N.M.M.R. and J.V.; **Supervision**: N.M.M.R. and J.V. All the authors have read and agreed to the published version of the manuscript.

Acknowledgements

This work was financially supported by project Project PTDC/ECI-CON/28766/2017—POCI-01-0145-FEDER-028766—funded by FEDER funds through COMPETE2020—Programa Operacional Competitividade e Internacionalização (POCI) and by national funds (PIDDAC) through FCT/MCTES, project Circular2B - 37_CALL#2 - Circular Construction in Energy-Efficient Modular Buildings funded by EEA Grants and by Base Funding—UIDB/04708/2020 of the CONSTRUCT—Instituto de I&D em Estruturas e Construções—funded by national funds through the FCT/MCTES (PIDDAC). R. C. Veloso and A. Souza would like to acknowledge the support of FCT—Fundação para

a Ciência e Tecnologia for the funding the doctoral grant SFRH/BD/148785/2019 and DFA/BD/8418/2020, respectively.

References

[1] A. Synnefa, M. Santamouris, H. Akbari, Estimating the effect of using cool coatings on energy loads and thermal comfort in residential buildings in various climatic conditions, Energy and Buildings, 39 (11) (2007) 1167-1174.

[2] M. Santamouris, A. Synnefa, T. Karlessi, Using advanced cool materials in the urban built environment to mitigate heat islands and improve thermal comfort conditions, Solar Energy, 85 (12) (2011) 3085-3102.

[3] N.M.M. Ramos, J. Maia, A.R. Souza, R.M.S.F. Almeida, L. Silva, Impact of Incorporating NIR Reflective Pigments in Finishing Coatings of ETICS, Infrastructures, 6 (6) (2021).

[4] M. Baneshi, S. Maruyama, A. Komiya, Comparison between aesthetic and thermal performances of copper oxide and titanium dioxide nano-particulate coatings, Journal of Quantitative Spectroscopy and Radiative Transfer, 112 (7) (2011) 1197-1204.

[5] A. Bishara, H. Kramberger-Kaplan, V. Ptatschek, Influence of different pigments on the facade surface temperatures, 11th Nordic Symposium on Building Physics (Nsb2017), 132 (2017) 447-453.

[6] N. Xie, H. Li, W.Z. Zhao, C. Zhang, B. Yang, H.J. Zhang, Y. Zhang, Optical and durability performance of near-infrared reflective coatings for cool pavement: Laboratorial investigation, Building and Environment, 163 (2019).

[7] C. Dias, R.C. Veloso, J. Maia, N.M.M. Ramos, J. Ventura, Oversight of radiative properties of coatings pigmented with TiO2 nanoparticles, Energy and Buildings, 271 (2022).

[8] R.C. Veloso, A. Souza, J. Maia, N.M.M. Ramos, J. Ventura, Nanomaterials with high solar reflectance as an emerging path towards energy-efficient envelope systems: a review, Journal of Materials Science, 56 (36) (2021) 19791-19839.

[9] S. Rossi, H. Lindmark, M. Fedel, Colored Paints Containing NIR-Reflective Pigments Exposed to Accelerated Ultraviolet Radiation Aging with Possible Application as Roof Coatings, Coatings, 10 (11) (2020).

[10] Y. Ma, Y. Chen, Z.F. Wang, H. Liu, Y.Y. Li, X.T. Wang, H.Y. Wei, G.J. Cheng, Controllable near-infrared reflectivity and infrared emissivity with substitutional iron-doped orthorhombic YMnO3 coatings, Solar Energy, 206 (2020) 778-786.

[11] S. Jose, A. Prakash, S. Laha, S. Natarajan, M.L. Reddy, Green colored nano-pigments derived from Y2BaCuO5: NIR reflective coatings, Dyes and Pigments, 107 (2014) 118-126.

[12] P. Jeevanandam, R.S. Mulukutla, M. Phillips, S. Chaudhuri, L.E. Erickson, K.J. Klabunde, Near Infrared Reflectance Properties of Metal Oxide Nanoparticles, The Journal of Physical Chemistry C, 111 (5) (2007) 1912-1918.

[13] Q. Gao, X. Wu, F. Shi, Novel superhydrophobic NIR reflective coatings based on Montmorillonite/SiO2 composites for Energy-saving building, Construction and Building Materials, 326 (2022) 126998.

[14] N.L. Alchapar, E.N. Correa, Aging of roof coatings. Solar reflectance stability according to their morphological characteristics, Construction and Building Materials, 102 (2016) 297-305.

[15] M. Zinzi, Characterisation and assessment of near infrared reflective paintings for building facade applications, Energy and Buildings, 114 (2016) 206-213.

[16] A.L. Pisello, V.L. Castaldo, C. Piselli, G. Pignatta, F. Cotana, Combined thermal effect of cool roof and cool facade on a prototype building, 6th International Building Physics Conference (Ibpc 2015), 78 (2015) 1556-1561.

[17] C. Vigneshkumar, Study on nanomaterials and application of nanotechnology and its impacts in construction., Discovery, 23 (75) (2014) 8-12.

[18] H. Boostani, S. Modirrousta, Review of Nanocoatings for Building Application, Icsdec 2016 - Integrating Data Science, Construction and Sustainability, 145 (2016) 1541-1548.

[19] H. Gonome, M. Baneshi, J. Okajima, A. Komiya, S. Maruyama, Controlling the radiative properties of cool black-color coatings pigmented with CuO submicron particles, Journal of Quantitative Spectroscopy & Radiative Transfer, 132 (2014) 90-98.

[20] E. Coser, V.F. Moritz, A. Krenzinger, C.A. Ferreira, Development of paints with infrared radiation reflective properties, Polimeros-Ciencia E Tecnologia, 25 (3) (2015) 305-310.

[21] D. Lof, G. Hamieau, M. Zalich, P. Ducher, S. Kynde, S.R. Midtgaard, C.F. Parasida, L. Arleth, G.V. Jensen, Dispersion state of TiO2 pigment particles studied by ultra-small-angle X-ray scattering revealing dependence on dispersant but limited change during drying of paint coating, Progress in Organic Coatings, 142 (2020).

[22] R. Paolini, D. Borroni, M. Pedeferri, M.V. Diamanti, Self-cleaning building materials: The multifaceted effects of titanium dioxide, Construction and Building Materials, 182 (2018) 126-133.

[23] J.H. Zhang, X.Y. Ren, D.N. Li, Z.Q. Dong, J.Q. Wang, L. Ren, B. Xue, F.F. Li, Enhanced ultraviolet shielding performances of TiO2 nanorods in different crystalline structures and illite-loaded composites, Colloids and Surfaces a-Physicochemical and Engineering Aspects, 608 (2021).

[24] F. Fang, Kennedy, J., Carder, D., Futter, J., Rubanov, S., Investigations of near infrared reflective behaviour of TiO2 nanopowders synthesized by arc discharg, Optical Materials, 36 (7) (2014) 1260-1265.

[25] M. Baneshi, H. Gonome, A. Komiya, S. Maruyama, The effect of particles size distribution on aesthetic and thermal performances of polydisperse TiO2 pigmented coatings: Comparison between numerical and experimental results, Journal of Quantitative Spectroscopy & Radiative Transfer, 113 (8) (2012a) 594-606.

[26] M. Baneshi, S. Maruyama, A. Komiya, The effects of TiO2 pigmented coatings characteristics on temperature and brightness of a coated black substrate, Solar Energy, 86 (1) (2012b) 200-207.

[27] M.K. Mehrizi, S.M. Mortazavi, S. Mallakpour, S.M. Bidoki, The Effect of Nano- and Micro-TiO2 Particles on Reflective Behavior of Printed Cotton/Nylon Fabrics in Vis/NIR Regions, Color Research and Application, 37 (3) (2012) 199-205.

[28] M. Baneshi, S. Maruyama, The impacts of applying typical and aesthetically-thermally optimized TiO2 pigmented coatings on cooling and heating load demands of a typical residential building in various climates of Iran, Energy and Buildings, 113 (2016) 99-111.

[29] Z. Yang, Y. Qi, J. Zhang, A novel perspective for reflective cooling composites: Influence of the difference between the effective refractive index of polymeric matrix and inorganic functional particles, Construction and Building Materials, 223 (2019) 928-938.

[30] L.W. Shen, Y.M. Zhang, P.G. Zhang, J.J. Shi, Z.M. Sun, Effect of TiO2 pigment gradation on the properties of thermal insulation coatings, International Journal of Minerals Metallurgy and Materials, 23 (12) (2016) 1466-1474.

[31] t. Chromaflo, Novapint D Solar Reflective Colorants, in, 2022.

[32] ASTM, ASTM E903: Standard Test Method for Solar Absorptance, Reflectance, and Transmittance of Materials Using Integrating Sphere, in, ASTM International, West Conshohocken, PA, USA, 2020.

[33] ASTM, ASTM G173: Standard Tables for Reference Solar Spectral Irradiances: Direct Normal and Hemispherical on 37° Tilted Surface, in, ASTM International, West Conshohocken, PA, USA, 2020.

[34] ASTM, ASTM G197-14: Standard Table for Reference Solar Spectral Distributions: Direct and Diffuse on 20° Tilted and Vertical Surfaces, in, ASTM International, West Conshohocken, PA, USA, 2021.

[35] ISO/CIE, ISO/CIE 11664: Colorimetry - Part 4: CIE 1976 L*a*b* Colour space., in, European Committe for Standardization, Brussels, 2007.

[36] L. Harynski, A. Olejnik, K. Grochowska, K. Siuzdak, A facile method for Tauc exponent and corresponding electronic transitions determination in semiconductors directly from UV-Vis spectroscopy data, Optical Materials, 127 (2022).

[37] A.B. Murphy, Band-gap determination from diffuse reflectance measurements of semiconductor films, and application to photoelectrochemical water-splitting, Solar Energy Materials and Solar Cells, 91 (14) (2007) 1326-1337.

[38] N. Sangiorgi, L. Aversa, R. Tatti, R. Verucchi, A. Sanson, Spectrophotometric method for optical band gap and electronic transitions determination of semiconductor materials, Optical Materials, 64 (2017) 18-25.

[39] J. Tauc, Optical properties and electronic structure of amorphous Ge and Si, Materials Research Bulletin, 3 (1) (1968) 37-46.

[40] P. Makula, M. Pacia, W. Macyk, How To Correctly Determine the Band Gap Energy of Modified Semiconductor Photocatalysts Based on UV-Vis Spectra, Journal of Physical Chemistry Letters, 9 (23) (2018) 6814-6817.

[41] P. Kubelka, Munk. F., Ein Beitrag Zur Optik der Farbanstriche, Zeitschrift für Technische Physik 12 (1931) 593-601.

[42] H. Bi, S.D. Li, Y.C. Zhang, Y.W. Du, Ferromagnetic-like behavior of ultrafine NiO nanocrystallites, Journal of Magnetism and Magnetic Materials, 277 (3) (2004) 363-367.

[43] M.P. Proenca, C.T. Sousa, A.M. Pereira, P.B. Tavares, J. Ventura, M. Vazquez, J.P. Araujo, Size and surface effects on the magnetic properties of NiO nanoparticles, Phys Chem Chem Phys, 13 (20) (2011) 9561-9567.

[44] L.B. Jiang, S.Y. Zhou, J.J. Yang, H. Wang, H.B. Yu, H.Y. Chen, Y.L. Zhao, X.Z. Yuan, W. Chu, H. Li, Near-Infrared Light Responsive TiO2 for Efficient Solar Energy Utilization, Advanced Functional Materials, 32 (12) (2022).

[45] S. Landi, I.R. Segundo, E. Freitas, M. Vasilevskiy, J. Carneiro, C.J. Tavares, Use and misuse of the Kubelka-Munk function to obtain the band gap energy from diffuse reflectance measurements, Solid State Communications, 341 (2022).

[46] Y. Yu, X. Yang, Y. Zhao, X. Zhang, L. An, M. Huang, G. Chen, R. Zhang, Engineering the Band Gap States of the Rutile TiO(2) (110) Surface by Modulating the Active Heteroatom, Angew Chem Int Ed Engl, 57 (28) (2018) 8550-8554.

[47] P. Deak, B. Aradi, T. Frauenheim, Band Lineup and Charge Carrier Separation in Mixed Rutile-Anatase Systems, Journal of Physical Chemistry C, 115 (8) (2011) 3443-3446.

[48] D.Y. Zhang, S. Dong, Challenges in band alignment between semiconducting materials: A case of rutile and anatase TiO2, Progress in Natural Science-Materials International, 29 (3) (2019) 277-284.

[49] J.R. Chen, F.X. Qiu, W.Z. Xu, S.S. Cao, H.J. Zhu, Recent progress in enhancing photocatalytic efficiency of TiO2-based materials, Applied Catalysis a-General, 495 (2015) 131-140.

[50] S. Na-Phattalung, D.J. Harding, P. Pattanasattayavong, H. Kim, J. Lee, D.W. Hwang, T.D. Chung, J. Yu, Band gap narrowing of TiO2 nanoparticles: A passivated Co-doping approach for enhanced photocatalytic activity, Journal of Physics and Chemistry of Solids, 162 (2022).

[51] X.Q. Zhang, Y.H. Zhu, X.L. Yang, S.W. Wang, J.H. Shen, B.B. Lin, C.Z. Li, Enhanced visible light photocatalytic activity of interlayer-isolated triplex Ag@SiO2@TiO2 core-shell nanoparticles, Nanoscale, 5 (8) (2013) 3359-3366.

[52] Y.Y. Li, Y. Ma, W.Y. Liu, Z.F. Wang, H. Liu, X.T. Wang, H.Y. Wei, S.H. Zeng, N. Yi, G.J. Cheng, A promising inorganic YFeO3 pigments with high near-infrared reflectance and infrared emission, Solar Energy, 226 (2021) 180-191.

[53] N. Serpone, D. Lawless, R. Khairutdinov, Size Effects on the Photophysical Properties of Colloidal Anatase TiO2 Particles: Size Quantization versus Direct Transitions in This Indirect Semiconductor?, The Journal of Physical Chemistry, 99 (45) (1995) 16646-16654.

[54] H. Lin, C.P. Huang, W. Li, C. Ni, S.I. Shah, Y.-H. Tseng, Size dependency of nanocrystalline TiO2 on its optical property and photocatalytic reactivity exemplified by 2-chlorophenol, Applied Catalysis B: Environmental, 68 (1) (2006) 1-11.

[55] H. Peng, J. Li, Quantum Confinement and Electronic Properties of Rutile TiO2 Nanowires, The Journal of Physical Chemistry C, 112 (51) (2008) 20241-20245.

[56] C. Kormann, D.W. Bahnemann, M.R. Hoffmann, Preparation and characterization of quantum-size titanium dioxide, The Journal of Physical Chemistry, 92 (18) (1988) 5196-5201.

[57] M. Anpo, T. Shima, S. Kodama, Y. Kubokawa, Photocatalytic hydrogenation of propyne with water on small-particle titania: size quantization effects and reaction intermediates, The Journal of Physical Chemistry, 91 (16) (1987) 4305-4310.

[58] E. Joselevich, I. Willner, Photosensitization of Quantum-Size TiO2 Particles in Water-in-Oil Microemulsions, The Journal of Physical Chemistry, 98 (31) (1994) 7628-7635.

[59] S. Xu, J. Xu, J. Zhang, Surface topography and cooling effects in poly(vinyl chloride) (PVC)/titanium dioxide (TiO2) composites exposed to UV-irradiation, Iranian Polymer Journal, 27 (12) (2018) 1011-1022.

[60] S. Monteiro, A. Dias, A.M. Mendes, J.P. Mendes, A.C. Serra, N. Rocha, J.F.J. Coelho, F.D. Magalhães, Stabilization of nano-TiO2 aqueous dispersions with poly(ethylene glycol)-b-poly(4-vinyl pyridine) block copolymer and their incorporation in photocatalytic acrylic varnishes, Progress in Organic Coatings, 77 (11) (2014) 1741-1749.

[61] M.D. Chadwick, J.W. Goodwin, E.J. Lawson, P.D.A. Mills, B. Vincent, Surface charge properties of colloidal titanium dioxide in ethylene glycol and water, Colloids and Surfaces A: Physicochemical and Engineering Aspects, 203 (1) (2002) 229-236.

[62] S.H. Othman, S. Abdul Rashid, T.I. Mohd Ghazi, N. Abdullah, Dispersion and Stabilization of Photocatalytic TiO₂ Nanoparticles in Aqueous Suspension for Coatings Applications, Journal of Nanomaterials, 2012 (2012) 718214.

[63] H.-Y. Tsai, S.-J. Chang, T.-Y. Yang, C.-C. Li, Distinct dispersion stability of various TiO2 nanopowders using ammonium polyacrylate as dispersant, Ceramics International, 44 (5) (2018) 5131-5138.

[64] M.P. Diebold, Optimizing the benefits of TiO2 in paints, Journal of Coatings Technology and Research, 17 (1) (2020) 1-17.

[65] M.K. Mehrizi, S.M. Mortazavi, S. Mallakpour, S.M. Bidoki, The effect of nano- and micro-TiO2 particles on reflective behavior of printed cotton/nylon fabrics in vis/NIR regions, Color Research & Application, 37 (3) (2012) 199-205.

[66] S. Fitzwater, Hook, JW, III,, Dependent Scattering Theory: A New Approach to Scattering in Paints., Journal of Coatings Technology 57 (1985) 39-47.

[67] J.H. Braun, A. Baidins, R.E. Marganski, TiO2 pigment technology: a review, Progress in Organic Coatings, 20 (2) (1992) 105-138.

[68] J.C. Auger, B. Stout, Dependent light scattering in white paint films: clarification and application of the theoretical concepts, Journal of Coatings Technology and Research, 9 (3) (2012) 287-295.

[69] J.-C. Auger, B. Stout, Discussion on dependent light scattering phenomenon in white paint films, Journal of Coatings Technology and Research, 10 (6) (2013) 929-931.

[70] M. Baneshi, S. Maruyama, H. Nakai, A. Komiya, A new approach to optimizing pigmented coatings considering both thermal and aesthetic effects, Journal of Quantitative Spectroscopy & Radiative Transfer, 110 (3) (2009) 192-204.

[71] M. Zinzi, E. Carnielo, G. Rossi, Directional and angular response of construction materials solar properties: Characterisation and assessment, Solar Energy, 115 (2015) 52-67.

[72] F.G. Cooper, in: Munsell Book of Color: Defining, Explaining, and Illustrating the Fundamental Characteristics of Color, Munsell Color Company, 1929.

[73] A.K.R. Choudhury, Chapter 2 - Scales for communicating colours,, in: Colour Measurement, In Woodhead Publishing Series in Textiles,, Woodhead Publishing,, 2010, pp. 19-69.

[74] C. Brothers, How To Choose A Paint Color Based On LRV, in.

[75] N.S. Gangakhedkar, Colour measurement of paint films and coatings, in: M.L. Gulrajani (Ed.) Colour Measurement, Woodhead Publishing, 2010, pp. 279-311.

[76] S. Sattar, Characterizing Color with Refletance, Journal of Chemical Education, 96 (6) (2019) 1124-1128.

[77] R. Oka, S. Iwasaki, T. Masui, Improvement of near-infrared (NIR) reflectivity and black color tone by doping Zn2+ into the Ca2Mn0.85Ti0.15O4 structure, RSC Advances, 9 (66) (2019) 38822-38827.

[78] N. Piri, A. Shams-Nateri, J. Mokhtari, Solar spectral performance of nanopigments, Solar Energy Materials and Solar Cells, 162 (2017) 72-82.

[79] N. Piri, A. Shams-Nateri, J. Mokhtari, The relationship between refractive index and optical properties of absorbing nanoparticle, Color Research and Application, 41 (5) (2016) 477-483.

[80] E.S. Cozza, M. Alloisio, A. Comite, G. Di Tanna, S. Vicini, NIR-reflecting properties of new paints for energy-efficient buildings, Solar Energy, 116 (2015) 108-116.

[81] W.S. Mokrzycki, M. Tatol, Colour Difference ΔE - a Survey, MG&V, 20 (4) (2011) 383-411.

[82] M.R.M. Izawa, E.A. Cloutis, T. Rhind, S.A. Mertzman, D.M. Applin, J.M. Stromberg, D.M. Sherman, Spectral reflectance properties of magnetites: Implications for remote sensing, Icarus, 319 (2019) 525-539.

Declaration of Competing Interest

The authors declare that they have no known competing financial interests or personal relationships that could have appeared to influence the work reported in this paper.

Cover Letter

IFIMUP—IN
Material Physics
Institute of the
University of Porto

CONSTRUCT

Rita Carvalho Veloso
Rua do Campo Alegre s/n
4169-007 Porto, Portugal
E-mail: up201001431@up.pt

Porto, 24 September 2023

Dear Editor,

We are pleased to submit herewith the manuscript entitled "*Unravelling the role of TiO_2 nanoparticles on the optical performance of dark colorants for coatings*" by Rita C. Veloso, Catarina Dias, Andrea Souza, Nuno M.M. Ramos and João Ventura to be considered for publication in Materials Chemistry and Physics Journal.

Buildings are currently responsible for more than 40% of the worldwide energy consumption and greenhouse gas emissions, and this trend is increasing. Thus, the assessment and enhancement buildings sustainability are becoming a major necessity for the consolidated development of the construction sector worldwide. Absorbed solar radiation increases the temperature of the building envelope system, which can also potentiate the early degradation of the façade coatings. This is mainly significant when dark tones are used for aesthetic purposes. One of the most promising solutions is to incorporate functional nanomaterials in the envelope system. The approach described in this work is based on a practical solution to incorporate TiO_2, one of the most effective nanopigments with excellent optical properties, in a conventional black colorant commonly used on façades. A systematic study was carried out to understand how the reflectance and colorimetry of the conventional black colorant vary depending on the intrinsic properties (size and concentration) of incorporated TiO_2 nanoparticles. Our study demonstrates that the reflective performance of these TiO_2-doped colorant is significantly improved (up to 86% increase in the NIR region). Furthermore, we observed that the most suitable TiO_2 concentration for enhancing the colorant properties is the 50 nm nanoparticles with 16% doping, showing 0.20 total reflectance when compared to only 0.13 for the conventional colorant. Our study can lead to new formulations of solar reflective coatings able to reduce overall cooling load particularly in warm climates with major cooling demands.

For all the above reasons, we believe that the topic of the manuscript is well suited to the scope and can be a quality contribution for the Journal.

Looking forward to hearing from you in due time,

Best regards,

Unravelling the role of TiO_2 nanoparticles on the optical performance of dark colorants for coatings

Rita Carvalho Veloso[1,2*], Catarina Dias[1], Andrea Souza[2], Nuno M. M. Ramos[2], João Ventura[1]

[1]IFIMUP, Departamento de Física e Astronomia, Faculdade de Ciências, Universidade do Porto, Rua do Campo Alegre s/n, 4169–007 Porto, Portugal

[2]CONSTRUCT-LFC, Departamento de Engenharia Civil, Faculdade de Engenharia, Universidade do Porto, Rua Dr. Roberto Frias, 4200-465 Porto, Portugal

* corresponding author details, up201001431@up.pt